Hydrogen atom formation from the photodissociation of water ice at 193 nm

Akihiro Yabushita, Yuichi Hashikawa, Atsushi Ikeda, and Masahiro Kawasaki
Department of Molecular Engineering, and Graduate School of Global Environmental Studies, Kyoto University, Kyoto 615-8510, Japan

Hiroto Tachikawa
Department of Molecular Chemistry, Graduate School of Engineering, Hokkaido University, Sapporo 060-8628, Japan

The TOF spectra of photofragment hydrogen atoms from the 193 nm photodissociation of amorphous ice at 90–140 K have been measured. The spectra consist of both a fast and a slow components that are characterized by average translational energies of $2k_BT_{trans}=0.39\pm0.04$ eV (2300 ± 200 K) and 0.02 eV (120 ± 20 K), respectively. The incident laser power dependency of the hydrogen atom production suggests one-photon process. The electronic excitation energy of a branched cluster, $(H_2O)_{6+1}$, has been theoretically calculated, where $(H_2O)_{6+1}$ is a $(H_2O)_6$ cyclic cluster attached by a water molecule with the hydrogen bond. The photoabsorption of this branched cluster is expected to appear at around 200 nm. The source of the hydrogen atoms is attributed to the photodissociation of the ice surface that is attached by water molecules with the hydrogen bond. Atmospheric implications are estimated for the photodissociation of the ice particles (Noctilucent clouds) at 190–230 nm in the region between 80 and 85 km altitude. © *2004 American Institute of Physics.* [DOI: 10.1063/1.1619939]

INTRODUCTION

Experimental and theoretical studies on the photodissociation of water have been extensively reported because of its importance to reaction dynamics and kinetics, atmospheric chemistry, astrophysics, etc.[1,2] A water molecule in the gas phase has the dissociation threshold of 5.1 eV to H+OH, while it has the first absorption band in the vacuum ultraviolet region below 185 nm (6.7 eV) and its absorption cross section at around 200 nm (6.2 eV) is very small, 10^{-23} cm^2.[3] The electronic transitions are of the Rydberg types.[4] The vertical transition at $\sim$200 nm requires excitation far into the classically forbidden regions of the OH stretch potential, where the ground state wave function amplitude is rapidly decaying.[5] In the condensed phase, due to the hydrogen-bonding among water molecules, the photoabsorption is blueshifted. The threshold for absorption spectra appears to be at 165 nm.[6,7] However, Dressler and Schnepp reported a region of weak and continuous absorption extending from 180 to 210 nm with a shallow maximum near 195 nm.[8] The absorption spectrum of polycrystalline hexagonal ice at the very tail in the range from 180 to 194 nm was measured at 263 K by Minton.[9] Since the intensity of this red-tailed band does not measurably increase with the water layer thickness, it may be relevant to *surface* water molecules and not to a cooled *bulk* ice. In this paper we have investigated the UV photodissociation dynamics of water ice at 193 and 248 nm with time-of-flight photofragment spectroscopy. Our purpose is to observe directly the formation of hydrogen atoms from the UV photodissociation of ice and estimate its influence on the mesosphere ozone depletion since there are appreciable amounts of small water–ice particles including the noctilucent clouds in the high-latitude mesopause region where the solar radiation at $\sim$200 nm is stronger than at the Lyman-α line.

AB INITIO THEORETICAL CALCULATIONS OF THE ELECTRONIC EXCITATION ENERGY OF A WATER MOLECULE ON A MODEL ICE SURFACE

In the present calculation, the structural model of an ice surface is constructed of cyclic six water molecules $(H_2O)_n$ ($n=6$), which is extracted from a structure of bulk ice. Its structure is fixed in the following calculations. Furthermore, one water molecule is connected by a hydrogen bond to the dangling OH group of the model water cluster. Here, this branched cluster is denoted by $(H_2O)_{6+1}$.[10] The position and structure of the added water molecule on the six-membered water cluster $(H_2O)_6$ were fully optimized by means of the HF/6-311++G(d,p) method.[11] The optimized structure of $(H_2O)_{6+1}$ is illustrated in Fig. 1. The oxygen–oxygen bond distance of the hydrogen bond was calculated to be 3.0967 Å. The water molecule is bound by the hydrogen bond (4.6 kcal mol^{-1}). Using a grazing-angle Fourier transform infrared reflection absorption spectroscopy, Zondlo *et al.* monitored the free OH stretch (or "dangling bond") in vapor-deposited H$_2$O-ice films between 94 and 120 K.[12] The temperature and pressure dependence of the dangling bond signal during film growth was used to estimate E_{dif} for H$_2$O on amorphous ice. They measured an upper limit of $E_{dif}=4.2\pm0.5$ kcal mol^{-1}, which is inconsistent with the bond energy for the water molecule on the model ice surface. For
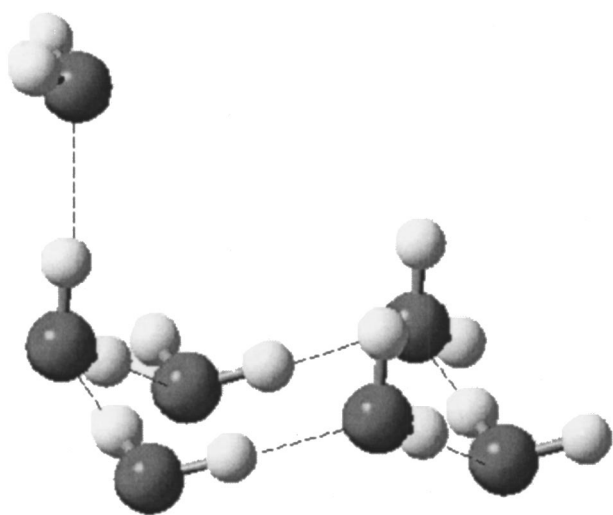
5463

FIG. 1. Optimized structure of a water molecule that is hydrogen-bonding to a model crystalline surface consisting of $(H_2O)_6$. The $(H_2O)_{6+1}$ water cluster is optimized at the HF/6-311++$G(d,p)$ level. Refer to Ref. 10.

a vapor-deposited water molecule on an water ice surface, a theoretical value for a barrier to diffusion (E_{dif}) was $E_{dif}=2.5-3$ kcal mol^{-1}.[13]

The electronic excitation energies were calculated by means of the complete active space multiconfiguration self-consistent field (CAS-SCF) method with a 6-311++$G(d,p)$ basis set.[14] Four electrons in four orbitals were considered as active electrons and active orbitals, respectively. At the CAS(4,4)/6-311++$G(d,p)$//MP2/6-311++$G(d,p)$ level, the first vertical excitation energy of $(H_2O)_{6+1}$ was calculated to be 6.62 eV, which is 0.11 eV lower than that of free H_2O (6.73 eV). The red shift is caused by an electron transfer from the hydrogen bond to the free (not hydrogen-bonded) hydrogen atom in the hydrogen-bond acceptor water molecule at the excited state. The charge of the hydrogen bonding H atom becomes partially positive, which is attracted by the negative charge of the oxygen atom of the hydrogen bond acceptor water molecule. Thus, the orbital energy is stabilized in the electronically excited state of the donor water molecule. As an additional test, we have calculated the first vertical excitation energies for water monomer, dimer, cyclic trimer, and cyclic tetramer: 6.73 eV for H_2O, 6.52 eV for $(H_2O)_2$, 7.05 eV for $(H_2O)_3$, 7.39 eV for $(H_2O)_4$. Furthermore, based on our calculation, we have found that the branched clusters have always smaller excitation energies than the corresponding cyclic clusters: 6.55 eV for $(H_2O)_{3+1}$, 6.84 eV for $(H_2O)_{4+1}$.

The cyclic trimer and tetramer have larger energies than the monomer. The dimer excitation energy is smaller than the monomer energy. This is in good agreement with the results reported by Harvey *et al.*[15] who calculated absorption line shapes of water clusters, $(H_2O)_n$, $n=2-6$. Their calculated UV spectra of the cyclic water clusters ($n=3-6$) indicate a strong blueshift with extended blue tails relative to the water monomer. Only in the case of the dimer, the absorption band appears at the red region. The redshifted absorption was attributed to the low excitation energy of the hydrogen-bond

donor water molecule because of its high polarizability in the excited state. All other water cyclic clusters larger than trimer exhibited a blueshift in the ultraviolet absorption bands because each water molecule is equally considered as a donor as well as an acceptor. An additional red tail appears only in the case of the dimer absorption band.[15] This red-tailed band arises from the hydrogen-bond donor H_2O molecule due to the wings in the ground state vibrational wave function that extend into the valleys of the dissociative excited state potential.

The blueshifted absorption spectra of cyclic water clusters are relevant to the vacuum UV absorption of bulk ice. The red absorption tail of the dimer is relevant to that of the vapor-deposited amorphous ice surface that is attached by water molecules. Thus, the amorphous water ice surface can have optical and structural characters similar to the water dimer.

EXPERIMENT

The experiments were performed in an ultrahigh vacuum chamber equipped with a pulsed gas source, excimer laser, and dye laser. The vacuum chamber was evacuated by two turbomolecular pumps in tandem (600 and 50 L s^{-1}). The base pressure was 0.5×10^{-8} Torr. A fused sapphire substrate was mounted on a liquid-nitrogen reservoir attached to a holder on an $X-Y-Z$ stage, and was heated by a tantalum filament (0.35 mm diam). The substrate temperature, T_{sub}, was controlled in the range 90–700 K, which was maintained within 1 K and was monitored with an Alumel–Chromel resistance thermometer attached into the sapphire substrate. The substrate was cleaned by oxygen atoms produced from the 193 nm photodissociation of gaseous NO_2 at $T_{sub}=520$ K for 60 min. This cleaning had no appreciable effect on the experimental results probably because the ice film thickness was more than a few hundred monolayers. However, when the probe laser light mistakenly hit the substrate surface, the experimental results were strongly affected probably because the growth of ice films were not uniform. The experimental details have been published elsewhere.[16]

A H_2O (or D_2O) ice film was prepared by deposition of water vapor on the sapphire substrate at $T_{sub}=90$ K with a pulsed gas head (General Valve, 10 Hz). A typical stagnation pressure of neat water vapor was 20 Torr. The state of water ice films is the porous amorphous solid water, which was prepared with the background deposition of water vapor at 90 K for 60 min, and then, annealed to the substrate temperature unless otherwise stated. The exposure was typically 1800 L (1 L$=1\times10^{-6}$ Torr s). This exposure resulted in formation of 600 ML of H_2O (or D_2O) on the substrate if we adopt the reported experimental conversion factor of 1 ML deposition by 3 L exposure,[17] which is in good agreement with 780 ML calculated kinematically for hexagonal crystalline density (1.1×10^{15} cm^{-2}),[18] collision velocity for 300 K gas and the sticking coefficient of unity.[19] The characteristics of the porous amorphous solid water are the existence of free OH groups and the porosity of the ice surface.[20]

Time-of-flight spectra of H (or D) atoms formed from the photodissociation of water ice were measured by the resonance-enhanced multiphoton ionization (REMPI) tech-
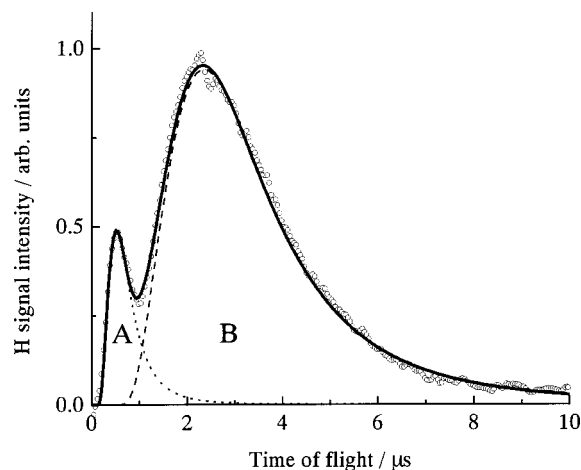
FIG. 2. A typical time-of-flight spectrum of H atoms from the 193 nm dissociation of amorphous ice at 90 K. The dotted curve and the broken curve are simulated ones for the Maxwell–Boltzmann velocity distributions with $(A)T_{trans}=2300$ K and $(B)T_{trans}=120$ K, respectively, using Eq. (1). This TOF spectrum is averaged over the entire Doppler profile of the REMPI spectrum of the H atom.
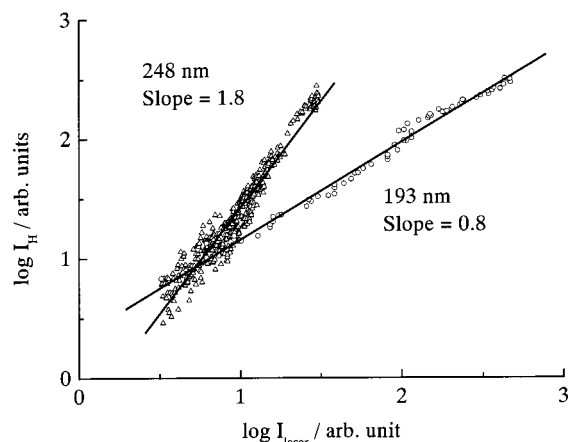

FIG. 3. Incident laser power dependencies of the H signal intensities at 193 or 248 nm, which were measured for the slow time-of-flight component B from amorphous ice at substrate temperature of 90 K. The slopes are 0.8 ± 0.1 for 193 nm and 1.6 ± 0.2 for 248 nm.

nique. A water ice film on the sapphire substrate (12 mm diameter) was photodissociated at 193 nm with an ArF excimer laser (Lambda Physik, COMPex, 10 Hz, typically reduced to 0.5 mJ cm^{-2} pulse^{-1} by optical filters) and at 248 nm with a KrF excimer laser (typically 2 mJ cm^{-2} pulse^{-1}). Neutral hydrogen atom photofragments produced by the photolysis laser pulse were ionized through a $(2+1)$ REMPI process at 243.1 nm with an Nd^{3+}:YAG laser pumped dye laser (Lambda Physik, SCANmate, 0.2 mJ pulse^{-1} at UV) with a lens ($f=0.20$ m). The subsequent REMPI signals of the atoms were detected by a homemade time-of-flight mass spectrometer. The distance between the substrate and the detection region was variable from 3 to 5 mm. It was usually set to 3 mm. TOF spectra were taken as a function of time delay, t, between the photolysis and probe laser pulses, which corresponds to the flight time between the substrate and the detection region.

EXPERIMENTAL RESULTS AND DISCUSSION

Figure 2 shows a typical TOF spectrum of H atoms from H$_2$O ice films at 90 K and 193 nm, which is a sum of the spectra measured at several Doppler shifts of the REMPI excitation spectrum. The TOF spectrum was fitted with $S(a,t,T_1,T_2)$, consisting of two flux weighted Maxwell–Boltzmann distributions defined by the translational temperature T_i and a coefficient, a,

$$S(a,t,T_1,T_2)=aS_{MB}(t,T_1)+(1-a)S_{MB}(t,T_2), \quad (1)$$

$$S_{MB}(t,r)=r^3t^{-4}\exp[-mr^2/(2k_BT_{trans}t^2)], \quad (2)$$

$$P_{MB}(E_t)=(k_BT_{trans})^{-2}E_t\exp[-E_t/(k_BT_{trans})], \quad (3)$$

where r is a flight length for the photofragment. $P_{MB}(E_t)$ is characterized by the average translational energy, $\langle E_t\rangle=2k_BT_{trans}$, where k_B is the Boltzmann constant, and T_{trans} is the translational temperature. Conversion from the energy distribution to the time-of-flight distribution was performed using the Jacobian listed by Zimmerman and Ho.[21] The an-

gular distribution of the photofragments is set to be flat because of rough surfaces of amorphous ice films. The TOF spectrum consists of both a fast component A and a slow component B, which are characterized by average translational energies of $2k_BT_{trans}=0.39\pm0.04$ eV $(2300\pm200$ K) and 0.02 eV $(120\pm20$ K), respectively. The slow component B is accommodated to the surface temperature prior to desorption.

As a function of laser intensity at 193 nm the REMPI intensity of the photofragment H atoms (B component) was measured at the peak TOF time. Incident laser power dependence of the signal intensity is 0.8 ± 0.1 as shown in Fig. 3, suggesting that H atoms are produced by a one-photon process. As a reference test, we performed 248 nm irradiation on an amorphous ice film at 90 K. Incident laser power dependence of the H signal intensity was 1.6 ± 0.2. These results suggest that the photodissociation at 248 nm is induced by a two-photon process. In the gas phase photolysis at 240–250 nm, the two-photon absorption to the third excited C($^1B_1$) state of water monomer was reported by Zhang et al.[22] The C($^1B_1$) state is bound near the Franck–Condon region but is predissociated by the B($^1A_1$) and A($^1B_1$) states.

Figure 4 shows the substrate temperature dependence of TOF spectra of H atoms from the 193 nm photodissociation of H$_2$O ice films, which are measured at the central wavelength of the REMPI Doppler profile. The H signal intensity decreased with increasing substrate temperatures from 110 to 140 K. Water ice forms an amorphous structure at substrate temperatures below 130 K.[17,23] Above 130 K, ice forms a cubic crystalline structure.[24] Since the phase change of amorphous ice to crystalline ice occurs at >120 K,[17] the decrease of the H atom signal intensity is caused by loss of amorphous nature of the ice film surface. According to our theoretical calculation about the branched cluster (H$_2$O)$_{6+1}$, it can have the red-tailed UV photoabsorption.

The inset of Fig. 4 shows TOF spectra of D atoms from the 193 nm photodissociation of the D$_2$O ice film with and without H$_2$O overlayers. After 30 L exposure of H$_2$O vapor over the amorphous D$_2$O ice film at 90 K, the fast TOF
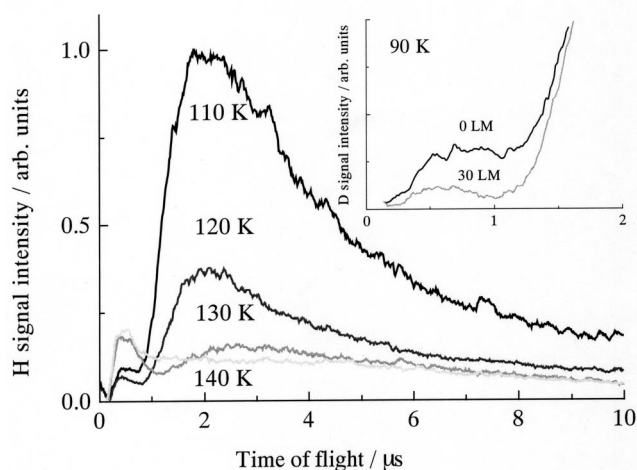
FIG. 4. Substrate temperature dependence of the time-of-flight (TOF) spectra of hydrogen atoms from the 193 nm photodissociation of ice. H_2O was first deposited on a substrate at 90 K, and then the substrate was heated stepwisely to the indicated (annealing) temperatures. The inset shows H_2O coverage dependence on the fast time-of-flight component of D atoms from the 193 nm photodissociation of amorphous D_2O ice at 90 K. TOF spectra of D atoms were measured from D_2O ice, (a) without exposure of the overlayer H_2O, and (b) with the overlayer H_2O exposed for 30 L. These TOF spectra are not averaged over the entire Doppler profile of the REMPI spectrum of the H atom, but the REMPI wavelength is fixed at the center wavelength of the Doppler profile.

component A of the D atoms disappeared, while the slow component B was not so affected at this exposure. These results indicate that the fast component A comes from the topmost D_2O layer of the ice film. The translational temperatures of the A and B components shown in Fig. 2 are consistent with this assumption, that is, H atoms from the topmost water molecules have a kinetic energy corresponding to $T_{trans} = 2300 \pm 200$ K. The H atoms of the B component have $T_{trans} = 120 \pm 20$ K that is close to the substrate temperature of 90–130 K. The slow component B is accommodated to the surface temperature prior to desorption. Kimmel *et al.* show for amorphous ice films that (a) the porosity decreases with the annealing temperature (90–130 K) and (b) the porosity stays nearly constant above 130 K.[18] In the present experiment, the relative ratios of the B component to the A component first decrease, and then stay constant with the substrate (annealing) temperature (Fig. 4). Thus, the B component could come partly from water molecules in the micropores of the ice film.

We have also measured the TOF spectra from the amorphous ice films prepared at three different ice growth temperatures (90, 100, and 110 K). In this case water vapor was deposited at the growth substrate temperature and the prepared film was photodissociated at the growth substrate temperature. The intensity ratio of the B component over the A component is smaller than the ratio observed for the ice film that was prepared at 90 K and then annealed to the same substrate temperature. According to Kimmel *et al.*,[18] the porosity is low for the ice films prepared at growth temperatures above 90 K. Thus, the origin of the B component is partly due to the photodissociation of the surface water molecules in the micropores. Since the temperature change induces not only the porosity change of the ice surface but also L- and D-defect concentration, etc. we need further experiments to confirm the origins of the temperature dependence observed in the TOF spectra.

COMPARISON WITH PREVIOUS WORKS

Several experimental studies on photodissociation of water adsorbed on cold surfaces were reported.[25–28] Wolf *et al.* performed UV irradiation of an H_2O bilayer adsorbed on Pd(111) at 95 K. For 6.4 or 5.0 eV irradiation, they found molecular desorption as well as dissociation of adsorbed molecules.[26] Both processes are due to electron transfer from the metal substrate to the layered water molecules and not related to direct photoabsorption process of the ice film. Nishi *et al.* reported a very weak signal of H atom from the 193 nm photodissociation of pure water ice adsorbed on the quartz plate with a signal to noise ratio of ~3 only when the laser beam was so strongly focused (0.5 J/cm^2) that two-photon excitation of H_2O molecules occurred.[28] In the present experiment, two-photon dissociation occurred at 248 nm with laser intensity of 2 mJ cm^{-2}, while the one-photon dissociation was observed at 193 nm and 0.5 mJ cm^{-2}. Because their laser intensity was stronger by over two orders of magnitude than our laser intensity, the one-photon dissociation process was smeared out by the two-photon process in their experiment.

About the dissociation threshold wavelength, Kimmel and Orlando measured D atoms from the electron-stimulated dissociation of amorphous D_2O ice adsorbed on Pt(111) at ~90 K.[29] They reported a low energy threshold for D atom production is 6–7 eV. There exists the dissociative electronic state near 200 nm. Their TOF spectra for D atoms consist of two components; one is ejected directly from the surface without interacting to surrounding molecules, and the other is accommodated to the surface temperature prior to desorption. These results are in good agreement with our TOF results. It is likely that the same electronic excitation and the dynamics occur in the photo- and electron bombardment dissociation.

ATMOSPHERIC IMPLICATIONS

The water vapor mixing ratio in the stratosphere and in the mesosphere of the Earth is maintained to be about 1–10 ppmv. Vardavas *et al.* have examined the role of H_2O photodissociation on ozone concentration in the upper atmosphere with emphasis on the region between 70 and 95 km altitude, where water vapor photodissociation by the solar Lyman-α line is considered to be the dominant source of H atoms that initiate the HOx cycle to decrease the O_3 mixing ratio.[30] Vertical ozone profiles obtained by HALOE[31] indicate that there is a deep minimum generated near the mesosphere at about 80 km. The depth of the minimum mixing ratio of O_3 is below 0.1 ppmv. Vertical ozone profiles and the H_2O volume mixing ratios given by the ATMOS observations[32] and the UARA/ISAMS observations[33] show a strong correlation between them. Those mixing ratios start becoming low at about 80 km. Therefore, the mesopause

ozone deep minimum is produced by the rapid destruction of water vapor by the solar Lyman-α line, and hence increase of HOx at altitudes between 80 and 85 km.

In the low temperature regions of the Earth's atmosphere, water molecules will cluster together to form ice particles that become visible when they have grown to about 50 nm in radius.[34–37] Noctilucent clouds (NLCs) are small water-ice particles, generated in the extremely cold (120–140 K) mesopause region near 88 km. Their most observable manifestation as thin (1–3 km) layers near 83 km is thought to be due to sedimentation downward from their height of origin, and growth by acquisition of water vapor in the denser regions. Lidar observations of ice crystals associated with NLCs have shown that a maximum column density is 10^{13} cm^{-2} at a radius of 0.02 μm.[38] About atmospheric implication of the present results, we have estimated the relative contribution of the ice particle photodissociation to the hydrogen atom formation near the high-latitude mesopause region, comparing with that of water vapor photodissociation,

$$H_i = \int d\lambda\, \sigma_i(\lambda) P_i(\lambda) \phi_i(\lambda) C_i,$$

where H_i denotes the amount of H atoms produced from ice and vapor photolysis, $\sigma(\lambda)$ absorption cross section at wavelength λ, and $P(\lambda)$ is the solar flux.[39] Water vapor is photodissociated at the Lyman-α line. The photon flux for vapor is set to P_{vapor} (121.6 nm) $= 3.6 \times 10^{11}$ photon cm^{-2} s^{-1}, which is the flux at solar minimum.[40] The photon flux for ice $P_{ice}(\lambda)$ will be discussed below. Since the absolute product quantum yield for the H atom production could not be measured in the present experiment, the yield is estimated as follows. The photodissociation quantum yield ϕ_{vapor} for water vapor is unity. ϕ_{ice} for ice could be larger than 0.04 that is taken from the reported yield (0.02) of hydrogen molecules from the *bulk* water ice photolysis in the vacuum UV.[41] It is smaller than unity since the *surface* water molecules that are hydrogen-bonding to the bulk ice surface are photodissociated. Hence, it would be reasonable to assume that ϕ_{ice} is 0.1. The average concentration $\langle C_{vapor} \rangle = 3.9 \times 10^9$ cm^{-3} of water vapor is taken from the reported mixing ratios (5–10 ppmV),[30,37] atmospheric temperatures (130–150 K) and pressure (0.01 mb) at a corresponding altitude of 80 km.[42] For NLC, the reported maximum column density of 10^{13} cm^{-2} and radius of 0.02 μm give effective spherical surface areas that can be irradiated by the solar radiation.[38] NLC particles have been shown to be nonspherical by recent polarization measurements and the surface of these particles is unlikely to be smooth.[43] The measured surface area of water ice films formed from the vapor phase at temperatures relevant to NLCs have surface areas up to 500 times larger than the geometric surface area of the substrate.[44] Murray and Plane, therefore, assumed that $A < 5 \times 10^{-5}$ cm^2, where A is the volumetric surface area (total aerosol surface area per unit volume of atmosphere).[45] Here we assume that the surface is uniformly covered by the hydrogen-bonding water molecules that have the red-tailed photoabsorption at 190–230 nm. Using the lattice constant for a crystalline ice surface, we calculated the number of the hydrogen-bonding

molecules that can absorb the solar radiation; $C_{ice} = 2.5 \times 10^{10}$ molecule cm^{-3}. In this calculation we assume that all H atoms pointing toward vacuum from the ice crystalline lattice are hydrogen-bonding to the O atoms of hydrogen-bond acceptor water molecules, which are the three hydrogen atoms pointing upward in Fig. 1. The hydrogen-bond donor water molecule absorbs UV light at 190–230 nm. The absorption cross section of the hydrogen-bond donor water molecule of the ice surface, $\langle \sigma_{ice}$ (190–230 nm)$\rangle = 1.6 \times 10^{-20}$ cm^2, is taken from the dimer absorption cross section calculated by Harvey *et al.*[15] The absorption cross section of water vapor, σ_{vapor}121.6 (nm) $= 5.4 \times 10^{-18}$ cm^2. The photon flux for ice $P_{ice}(\lambda)$ is effective in the region of $\lambda = 190$–230 nm, which is 1×10^{14} photon cm^{-2} s^{-1}. Using these parameters, the ratio of H_{ice}/H_{vapor} is estimated to be < 0.5, which indicates that the photodissociation of NLCs cannot be neglected in terms of the HOx cycle to ozone depletion near the high-latitude mesopause. This odd hydrogen reaction can also be applied to explain the loss of O atoms at 80 km altitude.[45]

ACKNOWLEDGMENTS

[1] R. Schinke, *Reaction Dynamics: Spectroscopy and Fragmentation of Small Polyatomic Molecules* (Cambridge University Press, Cambridge, 1995).

[2] H. Okabe, *Photochemistry of Small Molecules* (Wiley, New York, 1978).

[3] C-Y. Chung, E. P. Chew, B-M. Chen, M. Bahou, and Y-P. Lee, Nucl. Instrum. Methods Phys. Res. A **467**, 1572 (2001).

[4] O. Dutuit, A. Tabche-Fouhaile, I. Nenner, H. Frohlich, and P. M. Guyon, J. Chem. Phys. **83**, 584 (1985).

[5] D. F. Plusquellic, O. Votava, and D. J. Nesbitt, J. Chem. Phys. **107**, 6123 (1997).

[6] M. Seki, K. Kobayashi, and J. Nakahara, J. Chem. Phys. **50**, 2643 (1981).

[7] K. Kobayashi, J. Phys. Chem. **87**, 4317 (1983).

[8] K. Dressler and O. Schnepp, J. Chem. Phys. **33**, 270 (1960).

[9] A. P. Minton, J. Phys. Chem. **75**, 1162 (1971).

[10] When cyclic $(H_2O)_7$ is optimized, it forms a double ring structure consisting of a 3-membered ring plus a 4-membered ring.

[11] M. J. Frisch, G. W. Trucks, H. B. Schlegel *et al.*, *Ab initio* MO program, GAUSSIAN 98, Revision A.5, Gaussian, Inc., Pittsburgh, PA, 1998.

[12] M. A. Zondlo, T. B. Onasch, M. S. Warshawsky, M. A. Tolbert, G. Mallick, P. Arentz, and M. S. Robinson, J. Phys. Chem. B **101**, 10887 (1997).

[13] B. N. Hale, J. Kiefer, and C. A. Ward, J. Chem. Phys. **75**, 1991 (1981).

[14] M. J. Frisch, I. N. Ragazos, M. A. Robb, and H. B. Schlegel, Chem. Phys. Lett. **189**, 524 (1992).

[15] J. N. Harvey, J. O. Jung, and R. B. Gerber, J. Chem. Phys. **109**, 8747 (1998).

[16] A. Yabushita, Y. Inoue, T. Senga, M. Kawasaki, and S. Sato, J. Phys. Chem. B **106**, 3151 (2002).

[17] S. Sato, D. Yamaguchi, K. Nakagawa, Y. Inoue, A. Yabushita, and M. Kawasaki, Langmuir **16**, 9533 (2000).

[18] G. A. Kimmel, K. P. Stevenson, Z. Dohnálek, R. S. Smith, and B. D. Kay, J. Chem. Phys. **114**, 5284 (2001).

[19] D. E. Brown, S. M. George, C. Huang, E. K. L. Wong, K. B. Rider, R. S. Smith, and B. D. Kay, J. Phys. Chem. **100**, 4988 (1996).

[20] B. Rowland and J. P. Devlin, J. Chem. Phys. **94**, 812 (1991).

[21] F. M. Zimmermann and W. Ho, Surf. Sci. Rep. **22**, 127 (1995).

[22] J. Z. Zhang, E. H. Abramson, and D. G. Imre, J. Chem. Phys. **95**, 6536 (1991).

[23] W. Hagen, A. G. G. M. Tielens, and J. M. Greenberg, Chem. Phys. **56**, 367 (1981).

[24] D. Eisenberg and W. Kauzmann, *The Structure and Properties of Water* (Oxford University Press, New York, 1969).

[25] S. R. Baggott, K. W. Kolasinski, Luís M. A. Perdigão, M. A. Luis, D. Riedel, Q. Guo, and R. E. Palmer, J. Chem. Phys. **117**, 6667 (2002).

[26] M. Wolff, S. Nettesheim, J. M. White, E. Hasselbrink, and G. Ertl, J. Chem. Phys. **94**, 4610 (1991).

[27] P. A. Thiel and T. E. Madey, Surf. Sci. Rep. **7**, 211 (1987).

[28] N. Nishi, H. Shinohara, and T. Okuyama, J. Chem. Phys. **80**, 3898 (1984).

[29] G. A. Kimmel and T. M. Orlando, Phys. Rev. Lett. **75**, 2606 (1995).

[30] I. M. Vardavas, J. H. Carver, and F. W. Taylor, Ann. Geophys. **16**, 189 (1998).

[31] Halogen Occultation Experiment launched on UARS, in September 1991 as part of the Mission to Planet Earth, MTPE, Program.

[32] M. R. Gunson, C. B. Farmer, N. R. Norton, R. Zander, C. P. Rinsland, J. H. Shaw, and B. C. Gao, J. Geophys. Res. **95**, 13867 (1990).

[33] M. Goss-Custard, J. J. Remedios, A. Lambert *et al.*, J. Geophys. Res. **101**, 9907 (1996).

[34] G. E. Thomas and C. P. McKay, Planet. Space Sci. **33**, 1209 (1985).

[35] G. von Cossart, J. Fiedler, and U. von Zahn, Geophys. Res. Lett. **26**, 1513 (1999).

[36] M. Alpers, M. Gerding, J. Hoffner, and U. von Zahn, J. Geophys. Res. **105**, 12235 (2000).

[37] P. J. Espy and H. Jutt, J. Atmos. Sol.-Terr. Phys. **64**, 1823 (2002).

[38] L. Thomas, A. K. P. Marsh, D. P. Wareing, and M. A. Hassan, Geophys. Res. Lett. **21**, 385 (1994).

[39] G. P. Brasseur, J. J. Orlando, and G. S. Tyndall, *Atmospheric Chemistry and Global Change* (Oxford University Press, New York, 1999).

[40] T. N. Woods, W. K. Tobiska, G. J. Rottman, and J. R. Worden, J. Geophys. Res. **105**, 27195 (2000).

[41] N. Watanabe, T. Horii, and A. Kouchi, Astrophys. J. **541**, 772 (2000).

[42] J. M. Wallace and P. V. Hobbs, *Atmospheric Science* (Academic, New York, 1977).

[43] G. Baumgarten, K. H. Fricke, and G. T. von Cossart, Geophys. Res. Lett. **29**, 1630 (2002).

[44] F. J. Lübken, K. H. Fricke, and M. Langer, J. Geophys. Res. **101**, 9489 (1996).

[45] B. J. Murray and J. M. C. Plane, Adv. Space Res. **31**, 2075 (2003).